

Hysteretic transitions in the Kuramoto model with inertia

Simona Olmi,^{1,2} Adrian Navas,³ Stefano Boccaletti,^{1,2,3} and Alessandro Torcini^{1,2}

¹*CNR - Consiglio Nazionale delle Ricerche - Istituto dei Sistemi Complessi,
via Madonna del Piano 10, I-50019 Sesto Fiorentino, Italy*

²*INFN Sez. Firenze, via Sansone, 1 - I-50019 Sesto Fiorentino, Italy*

³*Centre for Biomedical Technology (UPM) 28922 Pozuelo de Alarcón, Madrid, Spain*

(Dated: December 8, 2021)

Abstract

We report finite size numerical investigations and mean field analysis of a Kuramoto model with inertia for fully coupled and diluted systems. In particular, we examine for a Gaussian distribution of the frequencies the transition from incoherence to coherence for increasingly large system size and inertia. For sufficiently large inertia the transition is hysteretic and within the hysteretic region clusters of locked oscillators of various sizes and different levels of synchronization coexist. A modification of the mean field theory developed by Tanaka, Lichtenberg, and Oishi [*Physica D*, 100 (1997) 279] allows to derive the synchronization profile associated to each of these clusters. We have also investigated numerically the **limits of existence** of the coherent and of the incoherent **solutions**. **The minimal coupling required to observe the coherent state is largely independent of the system size and it saturates to a constant value already for moderately large inertia values. The incoherent state is observable up to a critical coupling whose value saturates for large inertia and for finite system sizes, while in the thermodynamic limit this critical value diverges proportionally to the mass.** By increasing the inertia the transition becomes more complex, and the synchronization occurs via the emergence of clusters of whirling oscillators. The presence of these groups of coherently drifting oscillators induces oscillations in the order parameter. We have shown that the transition remains hysteretic even for randomly diluted networks up to a level of connectivity corresponding to few links per oscillator. Finally, an application to the Italian high-voltage power grid is reported, which reveals the emergence of quasi-periodic oscillations in the order parameter due to the simultaneous presence of many competing whirling clusters.

PACS numbers: 05.45.Xt, 05.45.-a, 64.60.aq, 89.75.-k

I. INTRODUCTION

Synchronization phenomena in phase oscillator networks are usually addressed by considering the paradigmatic Kuramoto model [1–4]. This model has been applied in many contexts ranging from crowd synchrony [5] to synchronization, learning and multistability in neuronal systems [6–8]. Furthermore, the model has been considered with different topologies ranging from homogeneous fully coupled networks to scale-free inhomogeneous systems [9]. Recently, it has been employed as a prototypical example to analyze low dimensional behaviour in a single large population of phase oscillators with a global sinusoidal coupling [10, 11], as well as in many hierarchically coupled sub-populations [12]. The study of the Kuramoto model for non-locally coupled arrays [13, 14] and for two populations of symmetrically globally coupled oscillators [15] lead to the discovery of the so-called Chimera states, whose existence has been revealed also experimentally in the very last years [16–19].

In this paper we will examine the dynamics and synchronization properties of a generalized Kuramoto model for phase oscillators with an inertial term both for fully coupled and for diluted systems. The modification of the Kuramoto model with an additional inertial term was firstly reported in [20, 21] by Tanaka, Lichtenberg and Oishi (TLO). These authors have been inspired in their modelization by a previous phase model developed by Ermentrout to mimic the synchronization mechanisms observed among the fireflies *Pteroptix Malacca* [22]. These fireflies synchronize their flashing activity by entraining to the forcing frequency with almost zero phase lag, even for stimulating frequencies different from their own intrinsic flashing frequency. The main ingredient to allow for the adaptation of the flashing frequency to the forcing one is to include an inertial term in a standard phase model for synchronization. Furthermore, networks of phase coupled oscillators with inertia have been recently employed to investigate the self-synchronization in power grids [23–25], as well as in disordered arrays of underdamped Josephson junctions [26]. Explosive synchronization have been reported for a complex system made of phase oscillators with inertia, where the natural frequency of each oscillator is assumed to be proportional to the degree of its node [27]. In particular, the authors have shown that the TLO mean field approach reproduces very well the numerical results for their system.

Our aim is to describe from a dynamical point of view the hysteretic transition observed in the TLO model for finite size systems and for various values of the inertia; we will

devote a particular emphasis to the description and characterization of coexisting clusters. Furthermore, the analysis is extended to random networks for different level of dilution and to a realistic case, represented by the high-voltage power grid in Italy. In particular, in Sect. II we will introduce the model and we will describe our simulation protocols as well as the order parameter employed to characterize the level of coherence in the system. The mean field theory developed by TLO is presented in Sect. III together with a generalization able to capture the emergence of clusters of locked oscillators of any size induced by the presence of the inertial term. The theoretical mean field results are compared with finite size simulations of fully coupled systems in Sect. IV; in the same Section the stability limits of the coherent and incoherent phase are numerically investigated for various simulation protocols as a function of the mass value and of the system size. A last subsection is devoted to the emergence of clusters of drifting oscillators and to their influence on the collective level of coherence. The hysteretic transition for random diluted networks is examined in the Sect. V. As a last point the behaviour of the model is analyzed for a network architecture corresponding to the Italian high-voltage power grid in Sect. VI. Finally, the reported results are briefly summarized and discussed in Sect. VII.

II. SIMULATION PROTOCOLS AND COHERENCE INDICATORS

By following Refs. [20, 21], we study the following version of the Kuramoto model with inertia:

$$m\ddot{\theta}_i + \dot{\theta}_i = \Omega_i + \frac{K}{N_i} \sum_j C_{i,j} \sin(\theta_j - \theta_i) \quad (1)$$

where θ_i and Ω_i are, respectively, the instantaneous phase and the natural frequency of the i -th oscillator, K is the coupling, the matrix element $C_{i,j}$ takes the value one (zero) depending if the link between oscillator i and j is present (absent) and N_i is the in-degree of the i -th oscillator. For a fully connected networks $C_{i,j} \equiv 1$ and $N_i = N$; for the diluted case we have considered undirected random graphs with a constant in-degree $N_i = N_c$, therefore each node has exactly N_c random connections and $C_{i,j} = C_{j,i}$. In the following we will mainly consider natural frequencies Ω_i randomly distributed according to a Gaussian distribution $g(\Omega) = \frac{1}{\sqrt{2\pi}} e^{-\Omega^2/2}$ with zero average and an unitary standard deviation.

To measure the level of coherence between the oscillators, we employ the complex order

parameter [28]

$$r(t)e^{i\phi(t)} = \frac{1}{N} \sum_j e^{i\theta_j} ; \quad (2)$$

where $r(t) \in [0 : 1]$ is the modulus and $\phi(t)$ the phase of the considered indicator. An asynchronous state, in a finite network, is characterized by $r \simeq \frac{1}{\sqrt{N}}$, while for $r \equiv 1$ the oscillators are fully synchronized and intermediate r -values correspond to partial synchronization. Another relevant indicator for the state of the network is the number of locked oscillators N_L , characterized by the same (vanishingly) small average phase velocity $\langle \dot{\theta}_i \rangle$, and the maximal locking frequency Ω_M , which corresponds to the maximal natural frequency $|\Omega_i|$ of the locked oscillators.

In general we will perform sequences of simulations **by varying adiabatically the coupling parameter K with two different protocols**. Namely, for the first protocol (I) the series of simulations is initialized for the decoupled system by considering random initial conditions for $\{\theta_i\}$ and $\{\dot{\theta}_i\}$. Afterwards the coupling is increased in steps ΔK until a maximal coupling K_M is reached. For each value of K , apart the very first one, the simulations is initialized by employing the last configuration of the previous simulation in the sequence. For the second protocol (II), starting from the final coupling K_M achieved **by employing** the protocol (I) simulation, the coupling is reduced in steps ΔK until $K = 0$ is recovered. At each step the system is simulated for a transient time T_R followed by a period T_W during which the average value of the order parameter \bar{r} and of the velocities $\{\langle \dot{\theta} \rangle\}$, as well as Ω_M , are estimated.

An example of the outcome obtained by performing the sequence of simulations of protocol (I) followed by protocol (II) is reported in Fig. 1 for not negligible inertia, namely, $m = 2$ and $m = 6$. During the first series of simulations (I) the system remains desynchronized up to a threshold $K = K_1^c \simeq 2$, above this value \bar{r} shows a jump to a finite value and then increases with K , saturating to $\bar{r} \simeq 1$ at sufficiently large coupling¹. By decreasing K one observes that the value of \bar{r} assumes larger values than during protocol (I), while the system desynchronizes at a smaller coupling, namely $K_2^c < K_1^c$. Therefore, the limit of stability of the asynchronous state is given by K_1^c , while the partially synchronized state can exist down to K_2^c , thus asynchronous and partially synchronous states coexist in the interval $[K_2^c; K_1^c]$.

The maximal locking frequency Ω_M increases with K during the first phase. In particular,

¹ Please notice that in the data shown in Fig. 1 the final state does not correspond to the 100% of synchronized oscillators, but to 99.6 % for $m = 2$ and 97.8 % for $m = 6$. However, the reported considerations are not modified by this minor discrepancy.

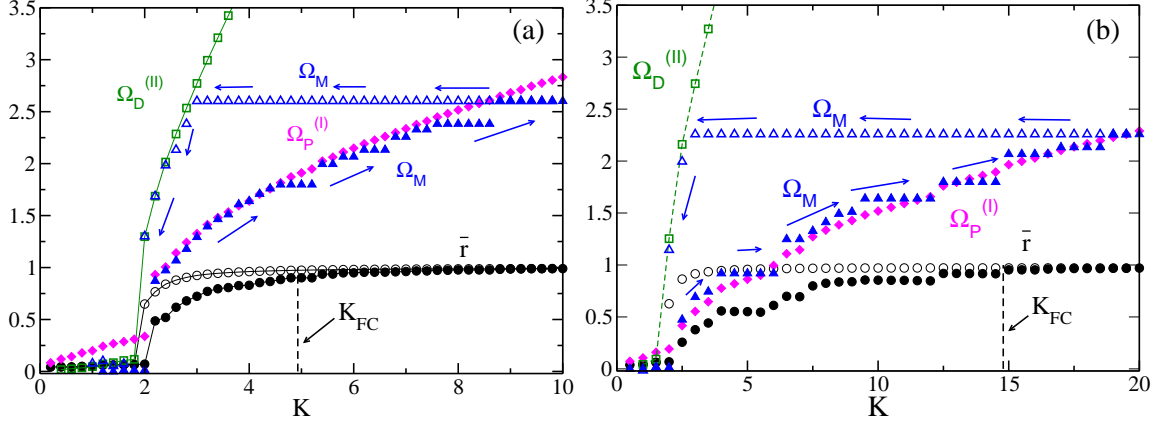


FIG. 1. (Color Online) Average order parameter \bar{r} (black circles) and maximal locking frequency Ω_M (blue triangles) as a function of the coupling K for two series of simulations performed following the protocol (I) (filled symbols) and the protocol (II) (empty symbols). The data refer to mass: $m = 2$ (a) and $m = 6$ (b). For $m = 2$ ($m = 6$) we set $\Delta K = 0.2$ ($\Delta K = 0.5$) and $K_M = 10$ ($K_M = 20$), in both cases $N = 500$, $T_R = 5,000$ and $T_W = 200$. The (magenta) diamonds indicate $\Omega_P^{(I)} = \frac{4}{\pi} \sqrt{\frac{K\bar{r}}{m}}$ for protocol (I), the (green) squares $\Omega_D^{(II)} = K\bar{r}$ for protocol (II), and the (black) dashed vertical line the coupling constant K_{FC}^G , whose expression is reported in Eq. (14).

for sufficiently large coupling, Ω_M displays plateaus followed by jumps for large coupling: this indicates that the oscillators frequencies Ω_i are grouped in small clusters. Finally, for $\bar{r} \simeq 1$ the frequency Ω_M attains a maximal value. By reducing the coupling, following now the protocol (II), Ω_M remains stucked to such a value for a large K interval. Then Ω_M reveals a rapid decrease towards zero for small coupling $K \simeq K_2^c$. In the next Section, we will give an interpretation of this behaviour.

We will also perform a series of simulations with a different protocol (S), to test for the independence of the results reported for K_1^c and K_2^c from the chosen initial conditions. In particular, for a certain coupling K we consider an asynchronous initial condition and we *perturb* such a state by forcing all the neurons with natural frequency $|\Omega_i| < \omega_S$ to be locked. Namely, we initially set their velocities and phase to zero, then we let evolve the system for a transient time T_R followed by a period T_W during which \bar{r} and the other quantities of interest are measured. These simulations will be employed to identify the interval of coupling parameters over which the coherent and incoherent solutions can be numerically observed.

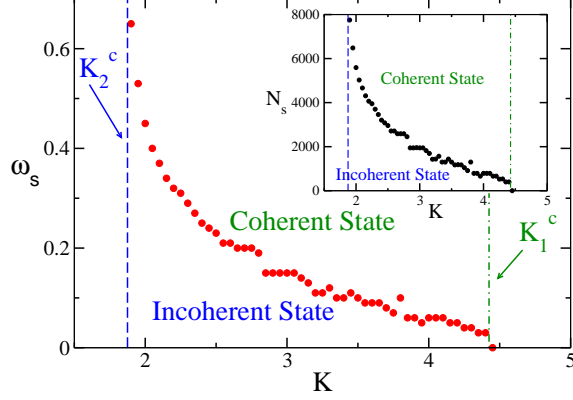


FIG. 2. (Color Online) Minimal ω_S giving rise to a state characterized by a finite level of synchronization (i.e. $\bar{r} > 0$) as a function of the coupling constant K . The inset reports the minimal number N_S of oscillators which should be initially locked in order to lead to the emergence of a coherent state, as a function of K . The vertical (green) dot-dashed line refers to the estimated K_1^c and the (blue) dashed line indicates the estimated K_2^c . The data refer to simulations performed with protocol (S) for $N = 16,000$, $m = 6$, with $T_W = 2,000$ and $T_R = 20,000$.

In more details, to measure with this approach K_1^c , which represents the upper coupling value for which the incoherent state can be observed, we fix the coupling K and we perform a series of simulations for increasing ω_S values, namely from $\omega_S = 0$ to $\omega_S = 3$ in steps $\Delta\omega_S = 0.05$. For each simulation we measure the order parameter \bar{r} , whenever it is finite for some $\omega_S > 0$, the corresponding coupling is associated to a partially synchronized state, the smallest coupling for which this occurs is identified as K_1^c .

In order to identify K_2^c , which is the lower value of the coupling for which the coherent state is numerically observable, we measure the minimal K for which the unperturbed asynchronous state (corresponding to $\omega_S = 0$) spontaneously evolves towards a partially synchronized solution. To give a statistically meaningful estimation of K_1^c and K_2^c , we have averaged the results obtained for various different initial conditions, ranging from 5 to 8, for all the considered system sizes and masses.

In principle, this approach cannot test rigorously for the stability of the coherent and incoherent states, since it deals with a very specific perturbation of the initial state. However, as we will show the estimations of the critical couplings obtained with protocol (S) coincide with those given by protocols (I) and (II), thus indicating that the reported results are not critically dependent on the chosen initial conditions.

III. MEAN FIELD THEORY

In the fully coupled case Eq. (1) can be rewritten, by employing the order parameter definition (2) as follows

$$m\ddot{\theta}_i + \dot{\theta}_i = \Omega_i - Kr \sin(\theta_i - \phi) \quad ; \quad (3)$$

which corresponds to a damped driven pendulum equation. This equation admits for sufficiently small forcing frequency Ω_i two fixed points: a stable node and a saddle. At larger frequencies $\Omega_i > \Omega_P \simeq \frac{4}{\pi} \sqrt{\frac{Kr}{m}}$ a homoclinic bifurcation leads to the emergence of a limit cycle from the saddle. The stable limit cycle and the stable fixed point coexist until a saddle node bifurcation, taking place at $\Omega_i = \Omega_D = Kr$, leads to the disappearance of the fixed points and for $\Omega_i > \Omega_D$ only the oscillating solution is presents. This scenario is correct for sufficiently large masses, at small m one have a direct transition from a stable node to a periodic oscillating orbit at $\Omega_i = \Omega_D = Kr$ [29].

Therefore for sufficiently large m there is a coexistence regime where, depending on the initial conditions, the single oscillator can rotate or stay quiet. How this single unit property will reflect in the self-consistent collective dynamics of the coupled systems is the topic of this paper.

A. The Theory of Tanaka, Lichtenberg, and Oishi

Tanaka, Lichtenberg, and Oishi in their seminal papers [20, 21] have examined the origin of the first order hysteretic transition observed for Lorentzian and flat (bounded) frequency distributions $g(\Omega)$ by considering two different initial states for the network : (I) the completely desynchronized state ($r = 0$) and (II) the fully synchronized one ($r \equiv 1$). Furthermore, in case I (II) they studied how the level of synchronization, measured by r , varies due to the increase (decrease) of the coupling K . In the first case the oscillators are all initially drifting with finite velocities $\langle \dot{\theta}_i \rangle$; by increasing K the oscillators with smaller natural frequencies $|\Omega_i| < \Omega_P$ begin to lock ($\langle \dot{\theta}_i \rangle = 0$), while the other continue to drift. This picture is confirmed by the data reported in Fig. 1, where the maximal value Ω_M of the frequencies of the locked oscillators is well approximated by Ω_P . **The process continues until all the oscillators are finally locked leading to $r = 1$.**

In the case (II), TLO assumed that initially all the oscillators were already locked, with an associated order parameter $r \equiv 1$. Therefore, the oscillators can start to drift only when the stable fixed point solution will disappear, leaving the system only with the limit cycle solution. This happens, by decreasing K , whenever $|\Omega_i| \geq \Omega_D = Kr$. This is numerically verified, indeed, as shown in Fig. 1, the maximal locked frequency Ω_M remains constant until, by decreasing K , it encounters the curve Ω_D and then Ω_M follows this latter curve down to the desynchronized state. The case (II) corresponds to the situation observable for the usual Kuramoto model, where there is no bistability [1].

In both the examined cases there is a group of desynchronized oscillators and one of locked oscillators separated by a frequency, Ω_P in the first case and Ω_D in the second one. These groups contribute differently to the total level of synchronization of the system, namely

$$r = r_L + r_D \quad (4)$$

where r_L (r_D) is the contribution of the locked (drifting) population.

For the locked population, one gets

$$r_L^{I,II} = Kr \int_{-\theta_{P,D}}^{\theta_{P,D}} \cos^2 \theta g(Kr \sin \theta) d\theta \quad ; \quad (5)$$

where $\theta_P = \sin^{-1}(\Omega_P/Kr)$ and $\theta_D = \sin^{-1}(\Omega_D/Kr) \equiv \pi/2$.

The drifting oscillators contribute to the total order parameter with a negative contribution; the self-consistent integral defining r_D **has been estimated by TLO** in a perturbative manner by performing an expansion up to the fourth order in $1/(mK)$ and $1/(m\Omega)$. **Therefore the obtained expression is correct in the limit of sufficiently large masses and it reads as**

$$r_D^{I,II} \simeq -mKr \int_{\Omega_{P,D}}^{\infty} \frac{1}{(m\Omega)^3} g(\Omega) d\Omega \quad ; \quad (6)$$

where $g(\Omega) = g(-\Omega)$.

By considering an initially desynchronized (fully synchronized) system and by increasing (decreasing) K one can get a theoretical approximation for the level of synchronization in the system by employing the mean-field expression (5), (6) and (4) for case I (II). In this way, two curves are obtained in the phase plane (K, r) , namely $r^I(K)$ and $r^{II}(K)$. In the following, we will show that these are not the unique admissible solutions in the mentioned plane, and these curves represent the lower and upper bound for the possible states characterized by a partial level of synchronization.

Let us notice that the expression for r_L and r_D reported in Eqs. (5) and (6) are the same for case (I) and (II), only the integration extrema have been changed. These are defined by the frequency which discriminates locked from drifting neuron, that in case (I) is Ω_P and in case (II) Ω_D . The value of these frequencies is a function of the order parameter r and of the coupling constant K , therefore by increasing (decreasing) K they change accordingly.

However, in principle one could fix the discriminating frequency to some arbitrary value Ω_0 and solve self-consistently the equations Eqs. (4), (5), and (6) for different values of the coupling K . This amounts to solve the following equation

$$\int_{-\theta_0}^{\theta_0} \cos^2 \theta g(Kr^0 \sin \theta) d\theta - m \int_{\Omega_0}^{\infty} \frac{1}{(m\Omega)^3} g(\Omega) d\Omega = \frac{1}{K} \quad ; \quad (7)$$

with $\theta_0 = \sin^{-1}(\Omega_0/Kr^0)$. Thus obtaining a solution $r^0 = r^0(K, \Omega_0)$, which exists provided that $\Omega_0 \leq \Omega_D(K) = r^0 K$. Therefore a portion of the (K, r) plane, delimited by the curve $r^{II}(K)$, will be filled with the curves $r_0(K)$ obtained for different Ω_0 values (as shown in Fig. 3 for fully coupled systems and in Fig. 14 for diluted ones.). These solutions represent clusters of N_L oscillators for which the maximal locking frequency and N_L do not vary upon changing the coupling strength. These states will be the subject of numerical investigation of the next Sections. In particular, we will show via numerical simulations that for $K > K_2^c$ these states are numerically observables within the portion of the phase space delimited by the two curves $r^I(K)$ and $r^{II}(K)$ (see Fig. 3 and Fig. 14).

B. Linear Stability Limit for the Incoherent Solution

As a final aspect, we will report the results of a recent theoretical mean field approach based on the Kramers description of the evolution of the single oscillator distributions for coupled oscillators with inertia and noise [30, 31]. In particular, the authors in [31] have derived an analytic expression for the coupling K_1^{MF} , which delimits the range of linear stability for the asynchronous state. In the limit of zero noise, K_1^{MF} can be obtained by solving the following equation

$$\frac{1}{K_1^{MF}} = \frac{\pi g(0)}{2} - \frac{m}{2} \int_{-\infty}^{\infty} \frac{g(\Omega) d\Omega}{1 + m^2 \Omega^2} \quad ; \quad (8)$$

where $g(\Omega)$ is an unimodal distribution of width σ . In the limit $m \rightarrow 0$ one recovers the value of the critical coupling for the usual Kuramoto model [1], namely $K_1^{MF}(m \equiv 0) = 2/(\pi g(0))$.

For a Lorentzian distribution an explicit expression for any value of the mass can be obtained

$$K_1^{MF} = 2\sigma(1 + m\sigma) \quad ; \quad (9)$$

which coincides with the one reported by Acebrón et al [30]. For a Gaussian distribution it is not possible to find an explicit expression for any m , however one can derive the first corrective terms to the zero mass limit, namely

$$K_1^{MF} = 2\sigma\sqrt{\frac{2}{\pi}} \left\{ 1 + \sqrt{\frac{2}{\pi}}m\sigma + \frac{2}{\pi}m^2\sigma^2 + \sqrt{\left(\frac{2}{\pi}\right)^3 - \frac{2}{\pi}m^3\sigma^3} \right\} + \mathcal{O}(m^4\sigma^4) \quad . \quad (10)$$

On the opposite limit one can analytically show that the critical coupling diverges as

$$K_1^{MF} \propto 2m\sigma^2 \quad \text{for} \quad m\sigma \rightarrow \infty \quad . \quad (11)$$

It can be seen that this scaling is already valid for not too large masses, indeed the analytical results obtained via Eq. (8) are very well approximated, in the range $m \in [1 : 30]$, by the following expression

$$K_1^{MF} \simeq 2\sigma(0.64 + m\sigma) \quad . \quad (12)$$

This result, together with Eq. (9), indicates that for both the Lorentzian and the Gaussian distribution the critical coupling diverges linearly with the mass and quadratically with the width of the frequency distribution.

In the next Section we will compare our numerical results for various system sizes with the mean-field result (8).

C. Limit of Complete Synchronization

Complete synchronization can be achieved, in the ideal case of infinite oscillators with a distribution $g(\Omega)$ with infinite support, only in the limit of infinite coupling. However, in finite systems an (almost) complete synchronization is attainable already at finite coupling, to give an estimation of this effective coupling K_{FC} one can proceed as follows. Let us estimate the pinning frequency $\bar{\Omega}_P$ required to have a large percentage of oscillators locked, this can be implicitly defined as, e.g.

$$\int_{-\bar{\Omega}_P}^{\bar{\Omega}_P} g(\Omega)d\Omega = 0.954 \quad ; \quad (13)$$

where by assuming $r \simeq 1$ one sets $\bar{\Omega}_P \simeq \frac{4}{\pi} \sqrt{\frac{K_{FC}}{m}}$ and from Eq. (13) one can derive the coupling K_{FC} . For a Gaussian distribution the integral reported in Eq. (13) amounts to consider two standard deviations, and therefore one gets

$$K_{FC}^G \simeq \left(\frac{\pi}{2}\right)^2 m \sigma^2 \quad ; \quad (14)$$

while for a Lorentzian distribution $g(\Omega) = \frac{\sigma}{\pi} \frac{1}{\sigma^2 + \Omega^2}$ this corresponds to

$$K_{FC}^L \simeq \left(\frac{13.815\pi}{4}\right)^2 m \sigma^2 \quad . \quad (15)$$

These results reveal that for increasing mass and width of the frequency distribution the system becomes harder and harder to fully synchronize and that to achieve the same level of synchronization a much larger coupling is required for the Lorentzian distribution (for the same m and σ).

IV. FULLY COUPLED SYSTEM

In this Section we will compare the analytical results with finite N simulations for the fully coupled system: a first comparison is reported in Fig. 3 for two different masses, namely $m = 2$ and $m = 6$. We observe that the data obtained by employing the procedure (II) are quite well reproduced from the mean field approximation r^{II} for both masses (solid red curve in Fig. 3). This is not the case for the theoretical estimation r^I (dashed red curve), which for $m = 2$ is larger than the numerical data up to quite large coupling, namely $K \simeq 5$; while for $m = 6$, a better agreement is observable at smaller K , however now \bar{r} reveals a step-wise structure for the data corresponding to protocol (I). This step-wise structure at large masses is due to the break down of the independence of the whirling oscillators: namely, to the formation of locked clusters at non zero velocities [20]. Therefore, oscillators join in small groups to the locked solution and not individually as it happens for smaller masses; this is clearly revealed by the behaviour of N_L versus the coupling K as reported in the insets of Fig. 3(b).

A. Hysteretic Behaviour

As already mentioned, we would like to better investigate the nature of the hysteresis observed by performing simulations accordingly to protocol (I) or protocol (II). In particular,

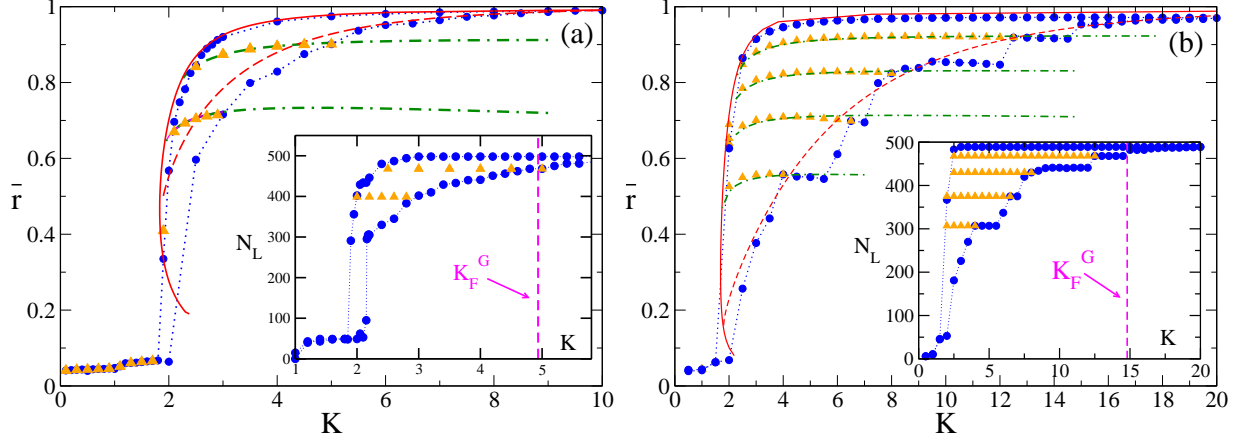


FIG. 3. (Color Online) Average order parameter \bar{r} versus the coupling constant K for $m = 2$ (a) and $m = 6$ (b). Mean field estimates: the dashed (solid) red curves refer to $r^I = r_L^I + r_D^I$ ($r^{II} = r_L^{II} + r_D^{II}$) as obtained by employing Eqs. (5) and (6) following protocol (I) (protocol (II)); the (green) dot-dashed curves are the solutions $r^0(K, \Omega_0)$ of Eq. (7) for different Ω_0 values. The employed values from bottom to top are: $\Omega_0 = 1.21$ and 1.71 in (a) and $\Omega_0 = 0.79, 1.09, 1.31$, and 1.79 in (b). Numerical simulations: (blue) filled circles have been obtained by following protocol (I) and then (II) starting from $K = 0$ until $K_M = 10$ ($K_M = 20$) for mass $m = 2$ ($m = 6$) with steps $\Delta K = 0.2$ ($\Delta K = 0.5$); (orange) filled triangles refer to simulations performed by starting from a final configuration obtained during protocol (I) and by decreasing the coupling from such initial configurations. The insets display N_L vs K for the numerical simulations reported in the main figures, the value of K_F^G (eq.(14)) is also reported in the two cases. The numerical data refer to $N = 500$, $T_R = 5000$, and $T_W = 200$.

we consider as initial condition a partially synchronized state obtained during protocol (I) for a certain coupling $K_S > K_1$, then we perform a sequence of consecutive simulations by reducing the coupling at regular steps ΔK . Some example of the obtained results are shown in Fig. 3, where we report \bar{r} and N_L measured during such simulations as a function of the coupling (orange filled triangles). From the simulations it is evident that the number of locked oscillators N_L remains constant until we do not reach the descending curve obtained with protocol (II). On the other hand \bar{r} decreases slightly with K , this decrease can be well approximated by the mean field solutions of Eq. (7), namely $r^0(K, \Omega_0)$ with $\Omega_0 = \Omega_P(K_S, r^I(K_S)) = \frac{4}{\pi} \sqrt{\frac{K_S r^I}{m}}$, see the green dot-dashed lines in Fig. 3 for $m = 2$ and $m = 6$. However, as soon as, by decreasing K , the frequency Ω_0 becomes equal or smaller than Ω_D ,

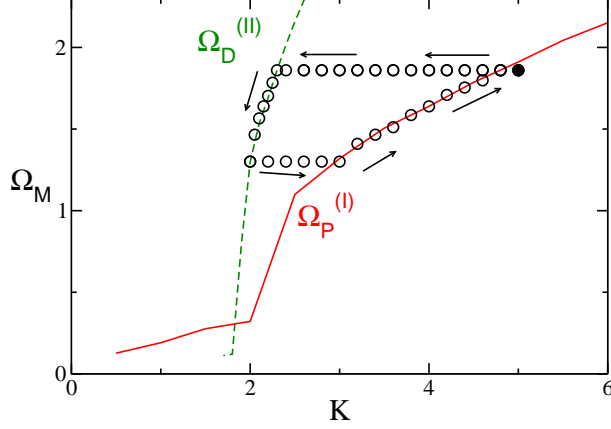


FIG. 4. (Color Online) Maximal locking frequency Ω_M versus the coupling constant K . The initial state is denoted by the filled circle at $K_I = 5$. The solid (red) curve indicates the frequency $\Omega_P^{(I)}$ and the dashed (green) curve the frequency $\Omega_D^{(II)}$. The numerical data refer to $N = 500$, $T_R = 5000$, $T_W = 200$, $m = 2$, and $\Delta K = 0.1 - 0.05$.

the order parameter has a rapid drop towards zero following the upper limit curve r^{II} .

To better interpret these results, let us focus on a simple numerical experiment. We consider a partially synchronized state obtained for $K_I = 5$ with $N = 500$ oscillators, then we first decrease the coupling in steps ΔK up to a coupling $K_F = 2$ and then we increase again K to return to the initial value K_I . During such cyclic simulation we measure Ω_M for each examined states, the results are reported in Fig. 4. It is clear that initially Ω_M does not vary and it remains identical to its initial value at $K_I = 5$. Furthermore, also the number of locked oscillators N_L remains constant. The maximal locking frequency (as well as N_L) starts to decrease with K only after Ω_M has reached the curve $\Omega_D^{(II)}$, then it follows exactly this curve, corresponding to protocol (II), until $K = K_F$. At this point we increase again the coupling: the measured Ω_M stays constant at the value $\Omega_D^{(II)} = 2 * r^{II}(K_F)$. The frequency Ω_M starts to increase only after its encounter with the curve $\Omega_P^{(I)}(K)$. In the final part of the simulation Ω_M recovers its initial value by following this latter curve. From these simulations it is clear that a synchronized cluster can be modified by varying the coupling, only by following protocol (I) or protocol (II), otherwise the coupling seems not to have any relevant effect on the cluster itself. In other words, all the states (K, Ω_M) contained between the curves $\Omega_D^{(II)}$ and $\Omega_P^{(I)}$ **are reachable** for the system dynamics, however they are quite peculiar.

We have verified that the path connecting the initial state at K_I to the curve $\Omega_D^{(II)}(K)$, as well as the one connecting K_F to the curve $\Omega_P^{(I)}(K)$, are completely reversible. We can increase (decrease) the coupling from K_I (K_F) up to any intermediate coupling value in steps of any size ΔK and then decrease (increase) the coupling to return to K_I (K_F) by performing the same steps and the system will pass exactly from the same states, characterized for each examined K by the values of \bar{r} and Ω_M . Furthermore, as mentioned, there is no dependence on the employed step ΔK , apart the restriction that the reached states should be contained within the phase space portion delimited by the two curves $\Omega_D^{(II)}$ and $\Omega_P^{(I)}$. As soon as the coupling variations would eventually lead the system outside this portion of the phase space, one should follow a hysteretic loop to return to the initial state, similar to the one reported in Fig. 4. Therefore, we can affirm that hysteretic loop of any size are possible within this region of the phase space. **For what concerns the stability of these states, we can only affirm that from a numerical point of view they appear to be stable within the considered integration times. However, a (linear) stability analysis of these solutions is required to confirm our numerical observations.**

B. Finite Size Effects

Let us now examine the influence of the system size on the studied transitions, in particular we will estimate the transition points K_1^c (K_2^c) by considering either a sequence of simulations obtained accordingly to protocol (I) (protocol (II)) or asynchronous (synchronous) initial conditions and by averaging over different realizations of the distributions of the forcing frequencies $\{\Omega_i\}$.

The results for the protocol (I) , protocol (II) simulations are reported in Fig. 5 for sizes ranging from $N = 500$ up to $N = 16,000$. It is immediately evident that K_2^c does not depend heavily on N , while the value of K_1^c is strongly influenced by the size of the system. Starting from the asynchronous state the system synchronizes at larger and larger coupling K_1^c with an associated jump in the order parameter which increases with N . Whenever the system starts to synchronize, then it follows reasonably well the mean field TLO prediction and this is particularly true on the way back towards the asynchronous state along the path associated to protocol (II) procedure. **However, TLO theory largely fails in giving an estimation of K_1^c for large system sizes, as shown in Fig. 5.**

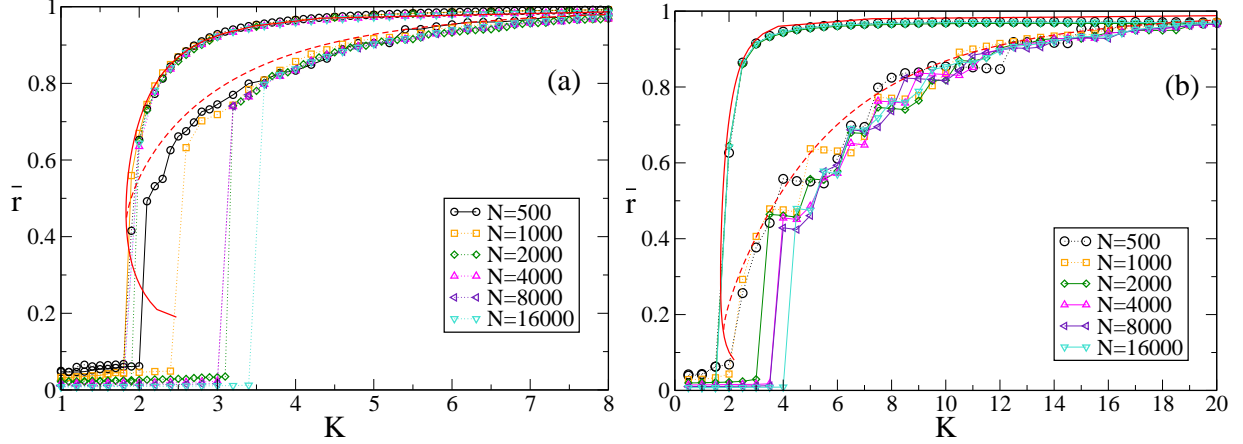


FIG. 5. (Color Online) Average order parameter \bar{r} versus the coupling constant K for various system sizes N : (a) $m = 2$ and (b) $m = 6$. The (red) solid and dashed curves are the theoretical estimates already reported in Fig. 3. The numerical data have been obtained by following protocol (I) and then protocol (II) from $K = 0$ up to $K_M = 10$ ($K_M = 20$) for mass $m = 2$ ($m = 6$) with $\Delta K = 0.2$ ($\Delta K = 0.5$). Data have been obtained by averaging the order parameter over a time window $T_W = 200$, after discarding a transient time $T_R \simeq 1,000 - 80,000$ depending on the system size, the larger T_R have been employed for the larger N .

In the following, we will analyze if the reported finite size results, and in particular the values of the critical couplings K_1^c and K_2^c , depend on the initial conditions and on the simulation protocols. For this analysis we focus on two masses, namely $m = 2$ and $m = 6$, and we consider system sizes ranging from $N = 500$ to $N = 16,000$. For each size and mass we evaluate K_1^c (K_2^c) by following protocol (I) (protocol (II)), as already shown in Fig. 5; furthermore now the critical coupling are also estimated by considering random initial conditions and by applying the protocol (S).

The results are reported in Fig. 6 for four different values of the mass; it is clear, by looking at the data displayed in Figs. 6(c) and (d), that protocol (I) (protocol (II)) and protocol (S) give essentially the same critical couplings, suggesting that their values are not dependent on the chosen initial conditions. Furthermore, while K_2^c reveals a weak dependence on N , K_1^c increases steadily with the system size. On the basis of our numerical data, it seems that the growth slow down at large N , but we are unable to judge if K_1^c is already saturated to an asymptotic value at the maximal reached system size, namely $N = 16,000$. To clarify this issue we compare our numerical results for K_1^c with the mean field estimated K_1^{MF} reported

in Eq. (8). The mean field result is always larger than the finite size measurements, however for small masses, namely $m = 0.8$ and $m = 1.0$, K_1^c seems to approach this asymptotic value already for the considered number of oscillators, as shown in Figs. 6(a) and (b). Therefore, in these two cases we attempt to identify the scaling law ruling the approach of K_1^c to its mean field value for increasing system sizes. The results reported in Fig. 7 suggest the following power law

$$[K_1^{MF} - K_1^c(N)] \propto N^{-\gamma} \quad ; \quad (16)$$

with $\gamma \simeq 0.22 - 0.23$.

Let us now consider several different values of the mass in the range $0.8 \leq m \leq 30$; the data for the critical couplings are reported in Fig 8 for different system sizes ranging from $N = 1,000$ to $N = 16,000$. It is evident that K_1^c grows with N for all masses, while K_2^c varies in a more limited manner. In particular, the estimated K_2^c shows an initial decrease with m followed by a constant plateau at larger masses (as shown in Fig 8 (b)). A possible mean field estimation for K_2^c can be given by the minimal value K_m^{II} reached by the coupling along the TLO curve $r^{II}(K)$. This value is reported in Fig 8 (b) together with the finite size data: at small masses K_m^{II} gives a reasonable approximation of the numerical data, while at larger masses it is always smaller than the finite size results and it saturates to a constant value for $m \rightarrow \infty$. These results indicate that finite size fluctuations destabilizes the coherent state at larger coupling than those expected from a mean field theory.

On the other hand K_1^c appears to increase with m up to some maximal value and then to decrease at large masses. However, this is clearly a finite size effect, since by increasing N the position of the maximum shifts to larger masses. The finite size curves $K_1^c = K_1^c(m, N)$ are always smaller than the mean field result K_1^{MF} (dashed orange line in Fig 8 (a)) for all considered system sizes and masses. However, as shown in the inset of Fig 8 (a), such curves collapse one over the other if the variables are properly rescaled, suggesting the following functional dependence

$$\xi \equiv \frac{K_1^{MF} - K_1^c(m, N)}{K_1^{MF}} = G\left(\frac{m}{N^\gamma}\right) \quad ; \quad (17)$$

where $\gamma = 1/5$. This result is consistent with the values of the scaling exponent γ found for fixed mass by fitting the data with the expression reported in Eq. (16). However, we are unable to provide any argument to justify such scaling and further analysis are required to interpret these results. A possible strategy could be to extend the approach reported in [32]

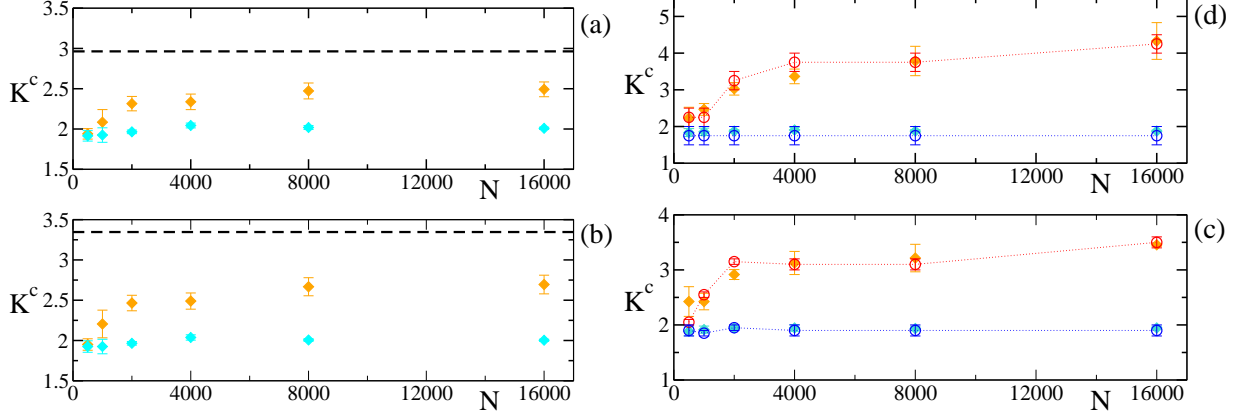


FIG. 6. (Color Online) Critical couplings K_1^c (orange filled diamonds and red empty circles) and K_2^c (cyan filled diamonds and blue empty circles) versus the system size N : (a) $m = 0.8$, (b) $m = 1$, (c) $m = 2$, and (d) $m = 6$. The filled symbols refer to estimates performed with protocol (S), while empty symbols, in panels (c) and (d), have been obtained with protocol (I) (protocol (II)) for K_1^c (K_2^c). The dashed (black) lines in panels (a) and (b) are the mean field values K_1^{MF} . This quantity is not reported in panels (c) and (d) for clarity reasons, due to its large value, namely, $K_1^{MF} = 5.31$ for $m = 2$ and $K_1^{MF} = 13.27$ for $m = 6$. For all panels the data have been derived by averaging in time over a window $T_W = 2,000$ and over 8 (5) different initial conditions for the protocol (S) (protocol (I) and (II)). For each simulation an initial transient time $T_R \simeq 20,000$ ($T_R \simeq 1,000 - 80,000$) has been discarded for protocol (S) (protocol (I) and (II)).

for the finite size analysis of the usual Kuramoto transition to the Kuramoto model with inertia.

C. Drifting Clusters

As already noticed in [20], for sufficiently large value of the mass one observes that the partially synchronized phase, obtained by following protocol (I), is characterized not only by the presence of the cluster of locked oscillators with $\langle \dot{\theta} \rangle \simeq 0$, but also by the emergence of clusters composed by drifting oscillators with finite average velocities. This is particularly clear in Fig. 9 (a), where we report the data for mass $m = 6$. By increasing the coupling K one observes for $K > 3$ the emergence of a cluster of whirling oscillators with a finite velocity $|\langle \dot{\theta} \rangle| \simeq 1.05$, these oscillators have natural frequencies in the range $|\Omega_i| \simeq 0.15 - 0.25$. The number of oscillators in this secondary cluster N_{DC} increases up to $K \simeq 5$, then it declines,

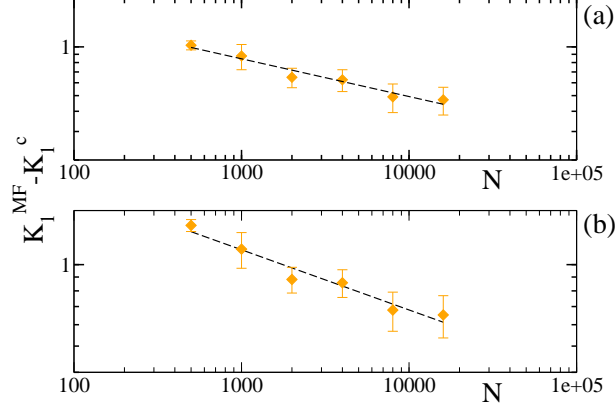


FIG. 7. (Color Online) The differences $K_1^{MF} - K_1^c(N)$ (filled orange diamonds) are reported versus the system size N for (a) $m = 0.8$ and (b) $m = 1$. The dashed (black) lines in both panels are power-law fits to the data: the difference vanishes as $0.42 \times N^{-0.23}$ for $m = 0.8$ (a) and as $5.27 \times N^{-0.22}$ for $m = 1$ (b). The data for K_1^c are the same reported in panel (a) and (b) in Fig. 6.

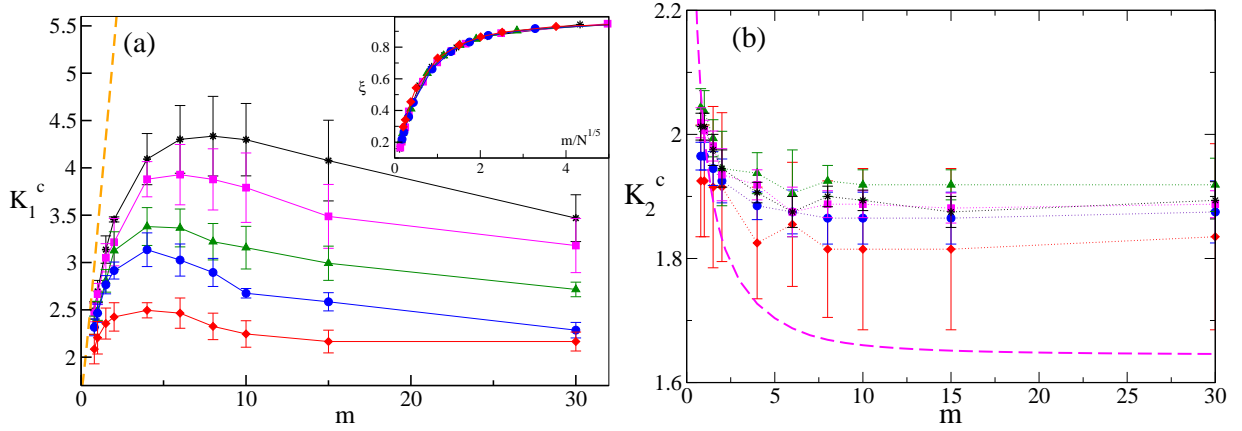


FIG. 8. (Color Online) Critical couplings K_1^c (a) and K_2^c (b) versus the mass m for different system sizes N . Namely, $N = 1,000$ (red diamond), $2,000$ (blue circles), $4,000$ (green triangles), $8,000$ (magenta squares) and $16,000$ (black asterisks). The dashed (orange) line in (a) is the mean field estimates K_1^{MF} ; while the dashed (magenta) line in (b) is the value K_m^{II} obtained by the TLO theory. The inset in panel (a) report the critical rescaled couplings $\xi = (K_1^{MF} - K_1^c)/K_1^{MF}$ as a function of $m/N^{1/5}$. The estimates have been obtained with protocol (S), by averaging in time over a window $T_W = 2,000 - 4,000$ and over 8 different initial conditions. For each simulation an initial transient time $T_R \simeq 20,000$ has been discarded.

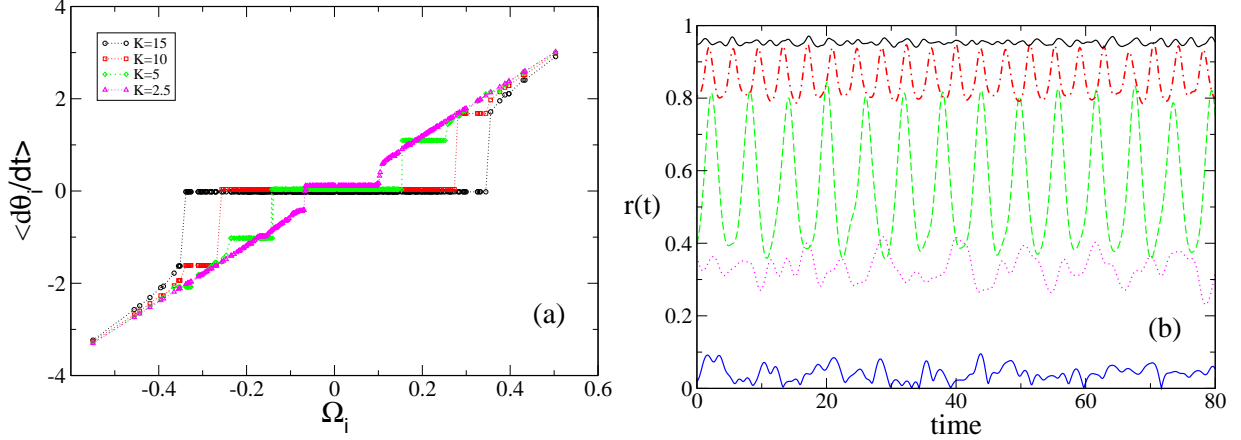


FIG. 9. (Color Online) (a) Average phase velocity $\langle \dot{\theta}_i \rangle$ of the oscillators versus their natural frequencies Ω_i : (magenta) triangles refer to $K = 2.5$, (green) diamond to $K = 5$, (red) squares to $K = 10$ and (black) circles to $K = 15$. For each simulation an initial transient $T_R \simeq 5,500$ has been discarded and the estimates have been obtained with protocol (I), by averaging in time over a window $T_W = 5,000$. (b) Order parameter $r(t)$ versus time for $m = 6$ and $N = 500$ and different coupling constants K : the (blue) solid curve corresponds to $K = 1$; the (magenta) dot-dashed line to $K = 2.5$, the (green) dashed line to $K = 5$, the (red) dashed line to $K = 10$ and the (black) solid line to $K = 15$. The data have been obtained by employing protocol (I) and for each simulation an initial transient time $T_R \simeq 1,500$ has been discarded and data are averaged over a time $T_W = 5000$.

finally the cluster is absorbed in the main locked group for $K \simeq 7$. At the same time a second smaller cluster emerges characterized by a larger average velocity $|\langle \dot{\theta} \rangle| \simeq 1.6$ (corresponding to larger $|\Omega_i| \simeq 0.27 - 0.34$). This second cluster merges with the locked oscillators for $K \simeq 12.5$, while a third one, composed of oscillators with even larger frequencies $|\Omega_i|$ and characterized by larger average phase velocity, arises. This process repeats until the full synchronization of the system is achieved.

The effect of these extra clusters on the collective dynamics is to induce oscillations in the temporal evolution of the order parameter, as one can see from Fig. 9 (b). In presence of drifting clusters characterized by the same average velocity (in absolute value), as for $m = 6$ and $K = 5$ in Fig. 9 (b), r exhibits almost regular oscillations and the period of these oscillations is related to the one associated to the oscillators in the whirling cluster. This can be appreciated from Fig. 10 (b), where we compare the evolution of the instantaneous

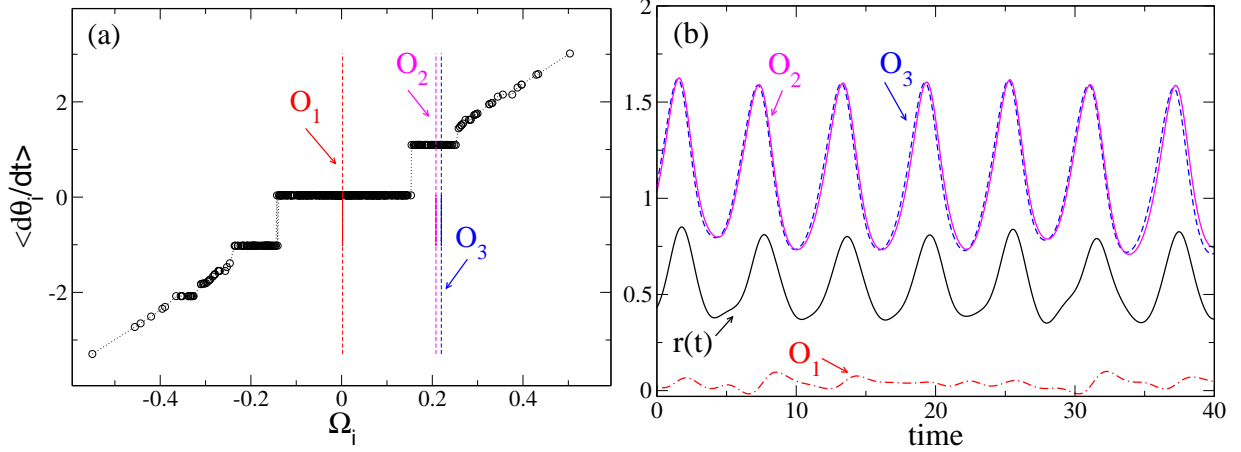


FIG. 10. (Color Online) (a) Average phase velocity $\langle \dot{\theta}_i \rangle$ of the oscillators versus the corresponding natural frequency Ω_i . The vertical dashed lines denote the three oscillators, O_1 , O_2 and O_3 , whose dynamical evolution is shown in (b). (b) The black curve represents the order parameter r versus time, the other curves refer to the time evolution of the phase velocities $\dot{\theta}(t)$ of the three oscillators O_1 (red dot-dashed curve), O_2 (magenta solid line) and O_3 (dashed blue curve). For each simulation an initial transient time $T_R \simeq 1,000$ has been discarded, the averages reported in (a) have been obtained over a time window $T_W = 20,000$. In both panels $K = 5$, $m = 6$ and $N = 500$.

velocity $\dot{\theta}_i$ for three oscillators and the time course of $r(t)$. We consider one oscillator O_1 in the locked cluster, and 2 oscillator O_2 and O_3 in the drifting cluster. We observe that these latter oscillators display essentially synchronized motions, while the phase velocity of O_1 oscillates irregularly around zero. Furthermore, the almost periodic oscillations of the order parameter $r(t)$ are clearly driven by the periodic oscillations of O_2 and O_3 (see Fig. 10 (b)).

We have also verified that the amplitude of the oscillations of $r(t)$ (measured as the difference between the maximal r_{max} and the minimal r_{min} value of the order parameter) and the number of oscillators in the drifting clusters N_{DC} correlates in an almost linear manner, as shown in Fig. 11 (b). Therefore we can conclude that the oscillations observable in the order parameter are induced by the presence of large secondary clusters characterized by finite whirling velocities. At smaller masses (e.g. $m = 2$) oscillations in the order parameter are present, but they are much more smaller and irregular (data not shown). These oscillations are probably due to finite size effects, since in this case we do not observe any cluster of drifting oscillators in the whole range from asynchronous to fully synchronized state.

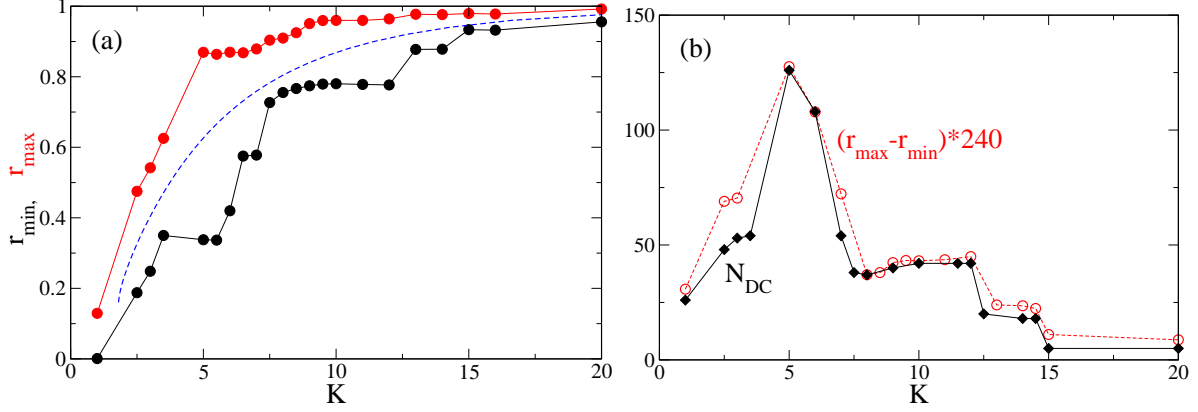


FIG. 11. (Color Online) (a) Minima and maxima of the order parameter r as a function of the coupling constant K . The (blue) dashed line refer to the theoretical estimate r^I , as obtained by employing Eqs. (5) and (6). (b) The number of oscillators in the drifting clusters N_{DC} (filled black diamond) is reported versus the coupling K together with the amplitude of the oscillations of the order parameter $r_{\max} - r_{\min}$ (empty red circles) rescaled by a factor 240. For each simulation an initial transient time $T_R \simeq 1,500$ has been discarded. The estimates have been obtained with protocol (I), by averaging in time over a window $T_W = 5000$, $m = 6$, $N = 500$.

The situation was quite different in the study reported in [21], where the authors considered natural frequencies $\{\Omega_i\}$ uniformly distributed over a finite interval and not Gaussian distributed as in the present study. In that case, by considering an initially clusterized state, similar to what done for protocol (S), $r(t)$ revealed regular oscillations even for masses as small as $m = 0.85$. In agreement with our results, the amplitude of the oscillations measured in [21] decreases by approaching the fully synchronized state (as shown in Fig.11). However, the authors in [21] did not relate the observed oscillations in $r(t)$ with the formation of drifting clusters.

As a final aspect, as one can appreciate from Fig. 5, for larger masses the discrepancies between the measured \bar{r} , obtained by employing protocol (I), and the theoretical mean field result r^I increase. In order to better investigate the origin of these discrepancies, we report in Fig.11 the minimal and maximal value of r as a function of the coupling K and we compare these values to the estimated mean field value r^I . The comparison clearly reveals that r^I is always contained between r_{\min} and r_{\max} , therefore the mean field theory captures correctly the average increase of the order parameter, but it is unable to foresee the oscillations in r . A new version of the theory developed by TLO in [20] is required in order to include also the

effect of clusters of whirling oscillators. A similar synchronization scenario, where oscillations in $r(t)$ are induced by the coexistence of several drifting clusters, has been recently reported for the Kuramoto model with degree assortativity [33].

V. DILUTED NETWORKS

In this Section we will analyze diluted neural networks obtained by considering random realizations of the coupling matrix $C_{i,j}$ with the constraints that the matrix should remain symmetric and the in-degree should be constant and equal to N_c ². In particular, we will examine if the introduction of the random dilution in the network will alter the results obtained by the mean-field theory and if the transition will remain hysteretic or not. For this analysis we limit ourselves to a single value of the mass, namely $m = 2$.

Let us first consider how the dependence of the order parameter \bar{r} on the coupling constant K will be modified in the diluted systems. In particular, we examine the outcomes of simulations performed with protocol (I) and (II) for a system size $N = 2,000$ and different realizations of the diluted network ranging from the fully coupled case to $N_c = 5$. The results, reported in Fig. 12, reveal that as far $N \geq 125$ (corresponding to the $\simeq 94\%$ of cutted links) it is difficult to distinguish among the fully coupled situation and the diluted ones. The small observed discrepancies can be due to finite size fluctuations. For larger dilution, the curves obtained with protocol (II) reveal a more rapid decay at larger coupling. Therefore K_2^c increases by decreasing N_c and approaches K_1^c as shown in Fig. 12 (b). The dilution has almost no effect on the curve obtained with protocol (I), in particular K_1^c remains unchanged (apart fluctuations within the error bars) until the percentage of incoming links N_c/N reduces below the 0.5%. For smaller connectivities both K_1^c and K_2^c shift to larger coupling and they approach one another, indicating that the synchronization transition from hysteretic tends to become continuous. Indeed this happens for $N = 1,000$ and $N = 500$ (as shown in the inset of Fig. 12 (b)): for such system sizes we observe essentially the same scenario as for $N = 2,000$, but already for in-degrees $N_c \leq 5$ the transition is no more hysteretic. This seems to suggest that by increasing the system size the transition

² In particular, each row i of the coupling matrix $C_{i,j}$ is generated by choosing randomly a node m and by imposing $C_{i,m} = C_{m,i} = 1$; this procedure is repeated until N_c elements of the row are set equal to one. Obviously, before accepting a new link, one should verify that in the considered row the number of links is smaller than N_c and that this is true also for all the interested columns. Finally, we have performed an iterative procedure to ensure that all rows and columns contain exactly N_c non zero elements.

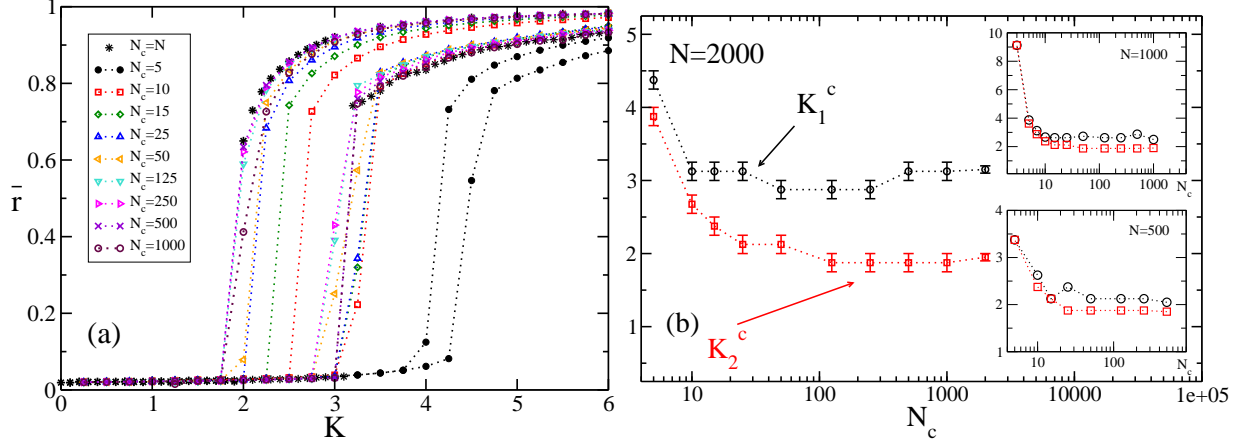


FIG. 12. (Color Online) (a) Average order parameter \bar{r} versus the coupling constant K for diluted neural networks for various N_c : 5 (filled black circles); 10 (red squares); 15 (green diamond); 25 (blue up triangles); 50 (orange left triangles); 125 (turquoise down triangles); 250 (right magenta triangles); 500 (violet crosses); 1,000 (empty maroon circles); 2,000 (black asterisks). (b) Critical constants K_1^c and K_2^c estimated for various values of the in-degree. The numerical data refer to $N = 2,000$; the upper inset refer to $N = 1,000$, the lower one to $N = 500$. For all simulations $m = 2$, $T_R = 10,000$, and $T_W = 2,000$; each series of simulations have been obtained by following protocol (I) and then (II) starting from $K = 0$ until $K_M = 20$ with steps $\Delta K = 0.25$. The reported data have been obtained by averaging over 10 - 20 different series of simulations, each corresponding to a different realization of the random network and of the distribution of the frequencies $\{\Omega_i\}$. The error bars in panel (b) correspond to $\Delta K/2$.

will stay hysteretic for vanishingly small percentages of connected (incoming) links. This is confirmed by the data shown in Fig. 13, where we report the width of the hysteretic loop W_h , measured at a fixed value of the order parameter, namely we considered $\bar{r} = 0.9$. For increasing system sizes W_h , measured for the same fraction of connected links N_c/N , increases, while the continuous transition, corresponding to $W_h \equiv 0$, is eventually reached for smaller and smaller value of N_c/N . Unfortunately, due to the CPU costs, we are unable to investigate in details diluted systems larger than $N = 2,000$.

Therefore, from this first analysis it emerges that the diluted or fully coupled systems, whenever the coupling is properly rescaled with the in-degree, as in Eq. 1, display the same phase diagram in the (\bar{r}, K) -plane even for very large dilution. In the following we will examine if the mean-field results obtained by following the TLO approach still apply to the

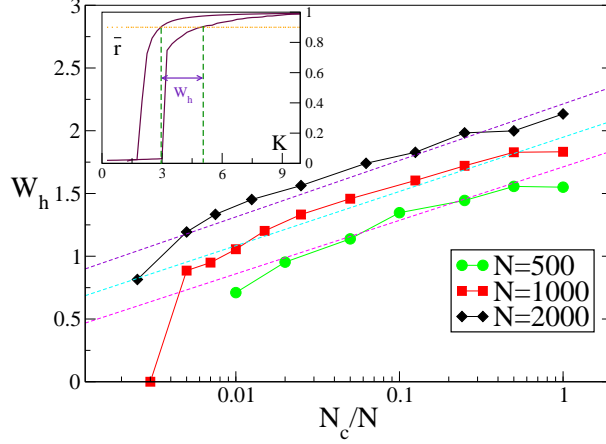


FIG. 13. (Color Online) Width of the hysteretic loop W_h , measured in correspondence of a order parameter value $\bar{r} = 0.9$, as a function of the percentage of connected links N_c/N . The (green) circles refer to $N = 500$, the (red) squares to $N = 1000$ and the (black) diamond to $N = 2,000$. The dashed lines refer to logarithmic fitting to the data in the range $0.01 < N_c/N \leq 1$. In the inset is graphically explained how W_h has been estimated, starting from one of the curves reported in Fig. 12 (a). The data refer to the same parameters and simulation protocols as in Fig. 12.

diluted system. The comparison reported in figure Fig. 14 confirms the good agreement between the numerical results obtained for a quite diluted system (namely, with 70 % of broken links) and the mean-field predictions (5) and (6). Furthermore, the data reported in Fig. 14 show that also in the diluted case all the states between the synchronization curves obtained following protocol (I) and protocol (II) are reachable and **numerically stable**, analogously to what shown in Subsect IV A for the fully coupled system. These states, displayed as orange filled triangles in Fig. 14, are characterized by a cluster composed by a constant number N_L of locked oscillators with frequencies smaller than a value Ω_M . The number of oscillators in the cluster N_L remains constant by varying the coupling between the two synchronization curves (I) and (II). Finally, the generalized mean-field solution $r^0(K, \Omega_0)$ (see Eq. (7)) is able, also in the diluted case, to well reproduce the numerically obtained paths connecting the synchronization curves (I) and (II) (see Fig. 14 and the inset).

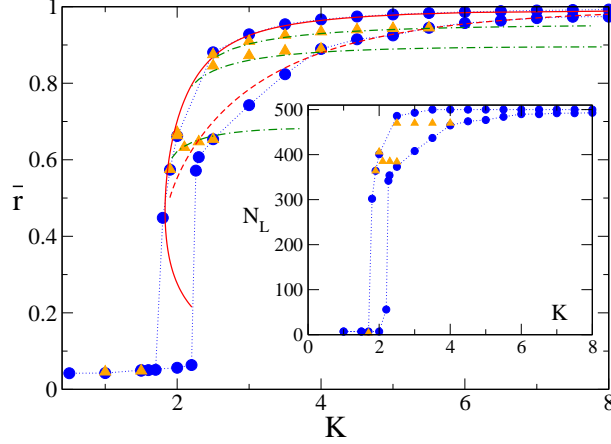


FIG. 14. (Color Online) Average order parameter \bar{r} versus the coupling constant K for a diluted network with 70% of cut links. Mean field estimates: the dashed (solid) red curves refer to $r^I = r_L^I + r_D^I$ ($r^{II} = r_L^{II} + r_D^{II}$) as obtained by employing Eqs. (5) and (6) following protocol I (protocol (II)); the (green) dot-dashed curves are the solutions $r^0(K, \Omega_0)$ of Eq. (7) for different Ω_0 values. The employed values from bottom to top are: $\Omega_0 = 2.05, 1.69$ and 1.10 . Numerical simulations: (blue) filled circles have been obtained by following protocol (I) and then (II) starting from $K = 0$ until $K_M = 20$ with steps $\Delta K = 0.5$; (orange) filled triangles refer to simulations performed by starting from a final configuration obtained during protocol (I) and by decreasing the coupling from such initial configurations. The insets display N_L vs K for the numerical simulations reported in the main figures. The numerical data refer to $m = 2$, $N = 500$, $N_c = 150$, $T_R = 5000$, and $T_W = 200$.

VI. A REALISTIC NETWORK: THE ITALIAN HIGH-VOLTAGE POWER GRID

In this Section, we examine if the previously reported features of the synchronization transition persist in a somehow more realistic setup. As we mentioned in the introduction a highly simplified model for a power grid composed of generators and consumers, resembling a Kuramoto model with inertia, can be obtained whenever the generator dynamics can be expressed in terms of the so-called swing equation [23, 24]. The self-synchronization emerging in this model has been recently object of investigation for different network topologies [25, 34, 35]. In this paper we will concentrate on the Italian high-voltage (380 kV) power grid (Sardinia excluded), which is composed of $N = 127$ nodes, divided in 34 sources (hydroelectric and thermal power plants) and 93 consumers, connected by 342 links [34]. This

network is characterized by a quite low average connectivity $\langle N_c \rangle = 2.865$, due to the geographical distributions of the nodes along Italy [36].

In this extremely simplified picture, each node can be described by its phase $\phi_i(t) = \omega_{AC}t + \theta_i(t)$, where $\omega_{AC} = 2\pi \times 50$ Hz or $2\pi \times 60$ Hz is the standard AC frequency and θ_i represents the phase deviation of the node i from the uniform rotation at frequency ω_{AC} . Furthermore, the equation of motion for each node is assumed to be the same for consumers and generators; these are distinguished by the sign of a quantity P_i associated each node: a positive (negative) P_i corresponds to generated (consumed) power. By employing the conservation of energy and by assuming that the grid operates in proximity of the AC frequency (i.e. $|\dot{\theta}| \ll \omega_{AC}$) and that the rate at which the energy is stored (in the kinetic term) is much smaller than the rate at which is dissipated, the evolution equations for the phase deviations take the following expression [24],

$$\ddot{\theta}_i = \alpha \left[-\dot{\theta}_i + P_i + K \sum_j C_{i,j} \sin(\theta_j - \theta_i) \right] . \quad (18)$$

To maintain a parallel with the previously studied model (1), we have multiplied the left-hand side by a term α , which in (18) represents the dissipations in the grid, while in (1) corresponds to the inverse of the mass. The parameter $\alpha \times K$ now represents the maximal power which can be transmitted between two connected nodes. More details on the model are reported in [23, 24, 35]. It is important to stress that in order to have a stable, fully locked state, as possible solution of (18), it is necessary that the sum of the generated power equal the sum of the consumed power. Thus, by assuming that all the generators are identical as well as all the consumers, the distribution of the P_i is made of two δ -function located at $P_i = -C$ and $P_i = +G$. In our simulations we have set $C = 1.0$, $G = 2.7353$ and $\alpha = 1/6$. This set-up corresponds to a Kuramoto model with inertia with a bimodal distribution of the frequencies.

As a first analysis we have performed simulations with protocol (I) for the model (18) by varying the parameter K and we have measured the corresponding average order parameter \bar{r} . As shown in Fig. 15 the behaviour of \bar{r} with K is non-monotonic. For small K the state is asynchronous with $\bar{r} \simeq 1/\sqrt{N}$, then \bar{r} shows an abrupt jump for $K \simeq 7$ to a finite value, then it decreases reaching a minimum at $K \simeq 9$. For larger K the order parameter increases steadily with K tending towards the fully synchronized regime.

This behaviour can be understood by examining the average phase velocity of the oscil-

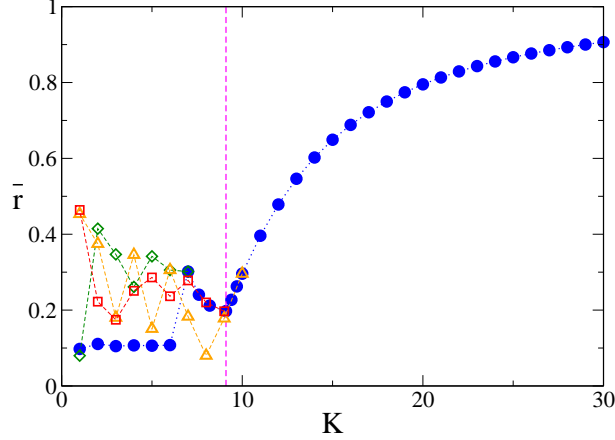


FIG. 15. (Color Online) Average order parameter \bar{r} versus the parameter K for the Italian high-voltage power grid network. The (blue) circles data have been obtained by following protocol (I) from $K = 1$ up to $K_M = 40$ with $\Delta K = 1$. The other symbols refer to simulations performed following protocol (II) starting from different initial coupling K_I down to $K = 1$, namely (orange) triangles $K_I = 10$, (red) squares $K_I = 9$ and (green) diamond $K_I = 7$. The dashed vertical (magenta) line indicates the value $K = 9$. The reported data have been obtained by averaging the order parameter over a time window $T_W = 5,000$, after discarding an initial transient time $T_R \simeq 60,000$. **The numerical data refer to $\alpha = 1/6$, $N=127$, $\langle N_c \rangle = 2.865$.**

lators $\langle \dot{\theta}_i \rangle$. As shown in Fig. 16, for coupling $K < 7$ the system is splitted in 2 clusters: one composed by the sources which oscillates with their proper frequency G and the other one containing the consumers, which rotates with average velocity $-C$. The oscillators in the two clusters rotate independently one from the other, therefore $\bar{r} \simeq 1/\sqrt{N}$. For $K \simeq 7$ the oscillators get entrained (as shown in Fig. 16) and most of them are locked with almost zero average velocity, however a large part (50 over 127) form a secondary cluster of whirling oscillators with a velocity $\langle \dot{\theta} \rangle \simeq -0.127$. This secondary cluster has a geographical origin, since it includes power stations and consumers located in the central part and south part of Italy, Sicily included. The presence of this whirling cluster induces large oscillations in the order parameter (see Fig. 18 (a)), reflecting almost regular transitions from a desynchronized to a partially synchronized state. By increasing the coupling to $K = 8$ the two clusters merge in an unique cluster with few scattered oscillators, however the average velocity is small but not zero, namely $\langle \dot{\theta} \rangle \simeq -0.05$ (as reported in Fig. 16). Therefore the average value of the order parameter \bar{r} decreases with respect to $K = 7$, where a large part of the oscillators

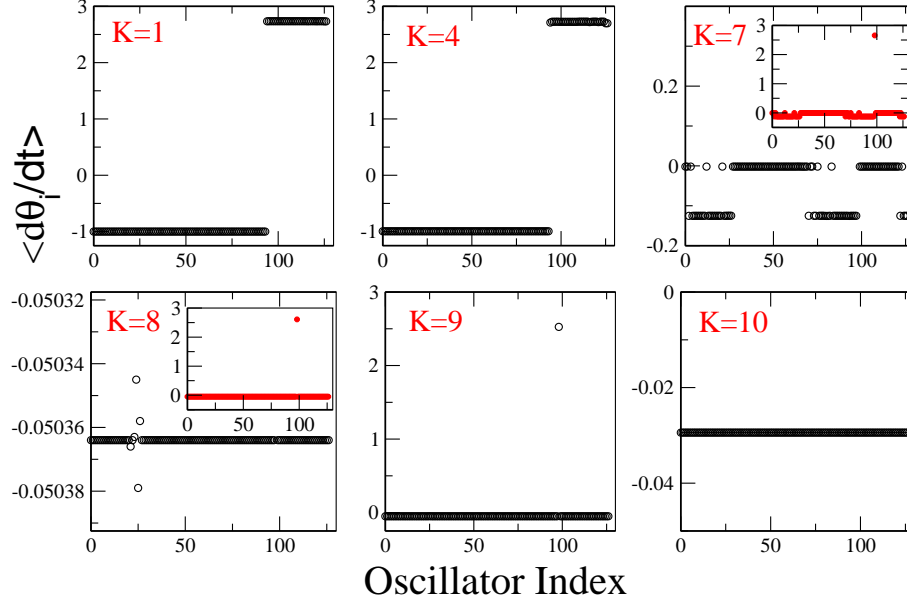


FIG. 16. (Color Online) Average phase velocity of each oscillator $\langle \dot{\theta}_i \rangle$ versus the oscillator index for different values of the coupling K . The oscillators have been reordered so that the first 93 are consumers and the last 34 sources. The data have been obtained by employing protocol (I), starting from zero coupling $K = 0$ and with $\Delta K = 1$. For each simulation an initial transient time $T_R \simeq 5,000$ has been discarded and the average is taken over a window $T_W = 5,000$. The numerical data refer to the same parameters as in Fig. 15.

was exactly locked. Up to $K = 9$, the really last node of the network, corresponding to one generator in Sicily connected with only one link to the rest of the Italian grid, still continues to oscillate independently from the other nodes, as shown in Fig. 16. Above $K = 9$ all the oscillators are finally locked in an unique cluster and the increase in the coupling is reflected in a monotonous increase in \bar{r} , similar to the one observed in standard Kuramoto models (see Fig. 15).

By applying protocol (II) we do not observe any hysteretic behaviour or multistability down to $K = 9$; instead for smaller coupling a quite intricate behaviour is observable. As shown in Fig. 17 starting from $K_I = 12$ and decreasing the coupling in steps of amplitude $\Delta K = 1$, the system stays mainly in one single cluster up to $K = 7$, apart the last node of the network which already detached from the network at some larger K . Indeed at $K = 7$ the order parameter has a constant value around 0.2 and no oscillations. As shown in Fig.18 (b), by decreasing the coupling to $K = 6$, wide oscillations emerge in $r(t)$ due to

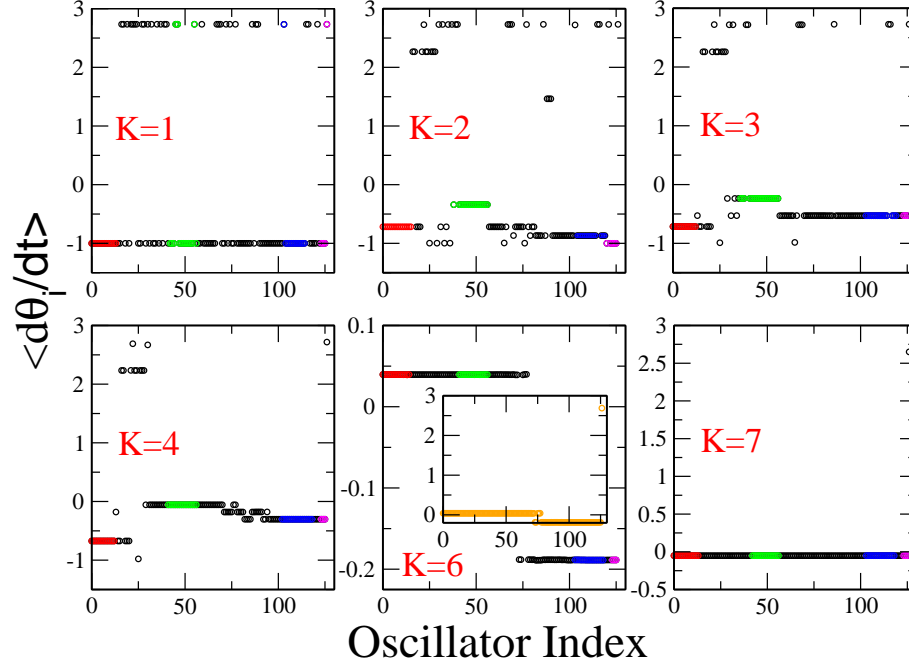


FIG. 17. (Color Online) Average phase velocity of each oscillator $\langle \dot{\theta}_i \rangle$ versus the corresponding oscillator index, ordered following the geographical distribution from north Italy to Sicily. The panels refer to different couplings. The colored clusters indicate Italian regions which remains connected for all the considered simulations: red symbols refer to Piedmont and Liguria; green symbols to Veneto and Friuli Venetia Giulia; blue symbols to Campania and Apulia; magenta symbols to Sicily. The data have been obtained by employing protocol (II) starting from $K_I = 12$ with $\Delta K = 1$ down to $K = 1$. For each simulation an initial transient time $T_R \simeq 50,000$ has been discarded and the averages performed over a window $T_W = 5000$. **The numerical data refer to the same parameters as in Fig. 15.**

the fact that the locked cluster has splitted in two clusters, the separation is similar to the one reported for $K = 7$ in Fig. 16. By further lowering K , several small whirling clusters appear and the behaviour of $r(t)$ becomes seemingly irregular for $2 \leq K \leq 5$ as reported in Fig.18 (b). An accurate analysis of the dynamics in terms of the maximal Lyapunov exponent has revealed that the irregular oscillations in $r(t)$ reflect quasi-periodic motions, since the measured maximal Lyapunov is always zero for the whole range of the considered couplings. **The presence of the inertial term, together with an architecture which favours a splitting based on the proximity of the oscillators, lead to the formation of several whirling clusters characterized by different average phase velocities.** The value of the order parameter

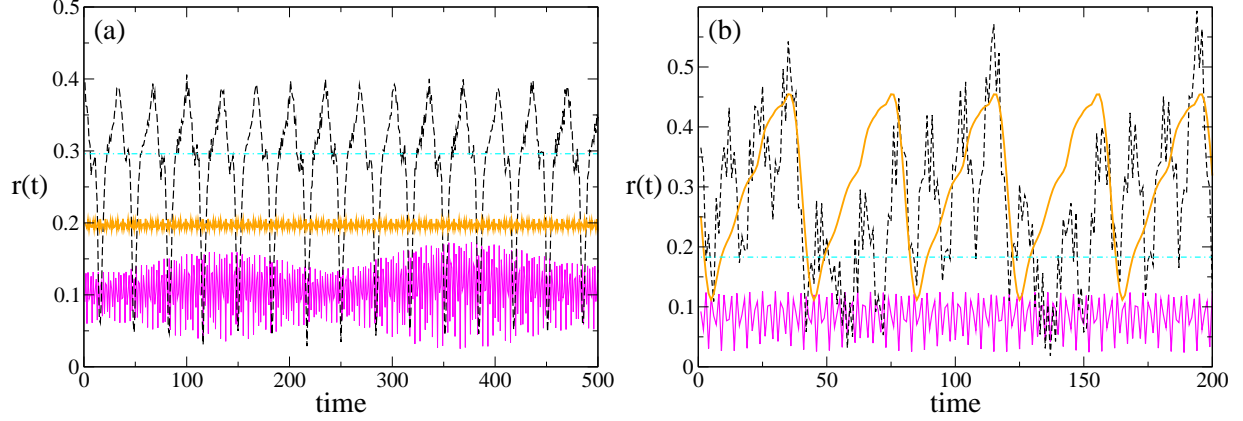


FIG. 18. (Color Online) Order parameter $r(t)$ versus time for the Italian high-voltage power grid network for different values of the parameter K . Panel (a): the dotted (magenta) curve corresponds to $K=4$; the dashed (black) line to $K=7$; the solid (orange) line to $K=9$; the dot-dashed (cyan) line to $K=10$. The data have been obtained by employing protocol (I) and for each simulation an initial transient time $T_R \simeq 5,000$ has been discarded. Panel (b): the solid (magenta) curve corresponds to $K=1$; the dashed (black) line to $K=4$; the solid (orange) thick line to $K=6$; the dot-dashed (cyan) line to $K=7$. The data have been obtained by employing protocol (II) and for each simulation an initial transient time $T_R \simeq 50,000$ has been discarded. The simulations refer to the same parameters employed in Fig. 15.

arises as a combination of these different contributions, each corresponding to a different oscillatory frequency. The splitting in different clusters is probably also at the origin of the multistability observed for $K < 7$: depending on the past history the grid splits in clusters formed by different groups of oscillators and this gives rise to different average values of the order parameter (see Fig. 15).

We have verified that the emergence of several whirling clusters, with an associated quasi-periodic behaviour of the order parameter, is observable also by considering an unimodal (Gaussian) distribution of the P_i . This confirms that the main ingredients at the origin of this phenomenon are the inertial term together with a short-range connectivity. Thus the bimodal distribution, here employed, seems not to be crucial and it can only lead to an enhancement of such effect.

VII. CONCLUSIONS

We have studied the synchronization transition for a globally coupled Kuramoto model with inertia for different system sizes and inertia values. The transition from incoherent to coherent state is hysteretic for sufficiently large masses. In particular, the upper value of the coupling constant (K_1^c), for which an incoherent state is observable, increases with the system sizes for all the examined masses. The estimated finite size value K_1^c has a non monotonic dependence on the mass m , exhibiting a maximum at some intermediate value of m . However, all the data obtained for different masses and sizes collapse onto an universal curve, whenever the distance of K_1^c with respect to its mean field value [31] is reported as a function of the mass divided by $N^{1/5}$. On the other hand, the coherent phase is attainable above a minimal critical coupling (K_2^c) which exhibits a weak dependence on the system size and it saturates to a constant asymptotic value for sufficiently large inertia values.

Furthermore, we have shown that clusters of locked oscillators of any size coexist within the hysteretic region. This region is delimited by two curves in the plane individuated by the coupling and the average value of the order parameter. Each curve corresponds to the *synchronization (desynchronization)* profile obtained starting from the fully desynchronized (synchronized) state. The original mean field theory developed by Tanaka, Lichtenberg, and Oishi in 1997 [20, 21] gives a reasonable estimate of both these limiting curves, while a generalization of such theory is capable to reproduce all the possible synchronization/desynchronization hysteretic loops. However, the TLO theory does not take into account the presence of clusters composed by drifting oscillators emerging for sufficiently large masses. The coexistence of these clusters with the cluster of locked oscillator induces oscillatory behaviour in the order parameter.

The properties of the hysteretic transition have been examined also for random diluted network; the main properties of the transition are not affected by the dilution up to extremely high values. The transition appears to become continuous only when the number of links per node becomes of the order of few units. By increasing the system size the transition to the continuous case (if any) shifts to smaller and smaller values of the connectivity.

In this paper we focused on Gaussian distribution of the natural frequencies, however we have obtained similar results also for Lorentzian distributions. It would be however interesting to examine how the transition modifies in presence of non-unimodal distributions

for the natural frequencies, like bimodal ones. Preliminary indications in this direction can be obtained by the reported analysis of the self-synchronization process occurring in the Italian high-voltage power grid, when the generators and consumers are mimicked in terms of a Kuramoto model with inertia [24]. In this case the transition is largely non hysteretic, probably this is due to the low value of the average connectivity in such a network. Coexistence of different states made of whirling and locked clusters, formed on regional basis, is observable only for electrical lines with a low value of the maximal transmissible power. These states are characterized by quasi-periodic oscillations in the order parameter due to the coexistence of several clusters of drifting oscillators.

A natural prosecution of the presented analysis would be the study of the stability of the observed clusters of locked and/or whirling oscillators **in presence of noise**. In this respect, exact mean-field results have been reported recently for fully coupled phase rotors with inertia and additive noise [31, 37]. However, the emergence of clusters in such systems has been not yet addressed neither on a theoretical basis nor via direct simulations.

ACKNOWLEDGMENTS

We acknowledge useful discussions with J. Almendral, M. Bär, I. Leyva, A. Pikovsky, J. Restrepo, S. Ruffo, and I Sendiña-Nadal, and we thank M. Frasca for providing the connectivity matrix relative to the Italian grid. Financial support has been given by the Italian Ministry of University and Research within the project CRISIS LAB PNR 2011-2013. SO and AT thank the German Science Foundation DFG, within the framework of SFB 910 "Control of self-organizing nonlinear systems", for the kind hospitality offered during 2012 and 2013 at Physikalisch-Technische Bundesanstalt in Berlin.

-
- [1] Y. Kuramoto, *Chemical oscillations, waves, and turbulence* (Courier Dover Publications, 2003).
 - [2] S. H. Strogatz, *Physica D: Nonlinear Phenomena* **143**, 1 (2000).
 - [3] A. Pikovsky, M. Rosenblum, and J. Kurths, *Synchronization: a universal concept in nonlinear sciences*, Vol. 12 (Cambridge university press, 2003).

- [4] J. A. Acebrón, L. L. Bonilla, C. J. P. Vicente, F. Ritort, and R. Spigler, *Reviews of modern physics* **77**, 137 (2005).
- [5] S. H. Strogatz, D. M. Abrams, A. McRobie, B. Eckhardt, and E. Ott, *Nature* **438**, 43 (2005).
- [6] D. Cumin and C. Unsworth, *Physica D: Nonlinear Phenomena* **226**, 181 (2007).
- [7] R. K. Niyogi and L. English, *Physical Review E* **80**, 066213 (2009).
- [8] Y. L. Maistrenko, B. Lysyansky, C. Hauptmann, O. Burylko, and P. A. Tass, *Physical Review E* **75**, 066207 (2007).
- [9] A. Arenas, A. Diaz-Guilera, J. Kurths, Y. Moreno, and C. Zhou, *Physics Reports* **469**, 93 (2008).
- [10] E. Ott and T. M. Antonsen, *Chaos: An Interdisciplinary Journal of Nonlinear Science* **18**, 037113 (2008).
- [11] S. A. Marvel, R. E. Mirollo, and S. H. Strogatz, *Chaos: An Interdisciplinary Journal of Nonlinear Science* **19**, 043104 (2009).
- [12] A. Pikovsky and M. Rosenblum, *Physical review letters* **101**, 264103 (2008).
- [13] Y. Kuramoto and D. Battogtokh, *NONLINEAR PHENOMENA IN COMPLEX SYSTEMS* **5**, 380 (2002).
- [14] D. M. Abrams and S. H. Strogatz, *Physical review letters* **93**, 174102 (2004).
- [15] D. M. Abrams, R. Mirollo, S. H. Strogatz, and D. A. Wiley, *Physical review letters* **101**, 084103 (2008).
- [16] A. M. Hagerstrom, T. E. Murphy, R. Roy, P. Hövel, I. Omelchenko, and E. Schöll, *Nature Physics* **8**, 658 (2012).
- [17] M. R. Tinsley, S. Nkomo, and K. Showalter, *Nature Physics* **8**, 662 (2012).
- [18] E. A. Martens, S. Thutupalli, A. Fourrière, and O. Hallatschek, *Proceedings of the National Academy of Sciences* **110**, 10563 (2013).
- [19] L. Larger, B. Penkovsky, and Y. Maistrenko, *Physical review letters* **111**, 054103 (2013).
- [20] H.-A. Tanaka, A. J. Lichtenberg, and S. Oishi, *Physical review letters* **78**, 2104 (1997).
- [21] H.-A. Tanaka, A. J. Lichtenberg, and S. Oishi, *Physica D: Nonlinear Phenomena* **100**, 279 (1997).
- [22] B. Ermentrout, *Journal of Mathematical Biology* **29**, 571 (1991).
- [23] F. Salam, J. E. Marsden, and P. P. Varaiya, *Circuits and Systems, IEEE Transactions on* **31**, 673 (1984).

- [24] G. Filatrella, A. H. Nielsen, and N. F. Pedersen, The European Physical Journal B **61**, 485 (2008).
- [25] M. Rohden, A. Sorge, M. Timme, and D. Witthaut, Physical review letters **109**, 064101 (2012).
- [26] B. Trees, V. Saranathan, and D. Stroud, Physical Review E **71**, 016215 (2005).
- [27] P. Ji, T. K. D. Peron, P. J. Menck, F. A. Rodrigues, and J. Kurths, Phys. Rev. Lett. **110**, 218701 (2013).
- [28] A. Winfree, *The Geometry of Biological Time* (Springer-Verlag, Berlin-Heidelberg-New York, 1980).
- [29] S. H. Strogatz, *Nonlinear dynamics and chaos (with applications to physics, biology, chemistry a* (Perseus Publishing, 2006).
- [30] J. Acebrón, L. Bonilla, and R. Spigler, Physical Review E **62**, 3437 (2000).
- [31] S. Gupta, A. Campa, and S. Ruffo, Physical Review E **89**, 022123 (2014).
- [32] H. Hong, H. Chaté, H. Park, and L.-H. Tang, Physical review letters **99**, 184101 (2007).
- [33] J. G. Restrepo and E. Ott, arXiv preprint arXiv:1407.5725 (2014).
- [34] L. Fortuna, M. Frasca, and A. Sarra Fiore, International Journal of Modern Physics B **26** (2012).
- [35] M. Rohden, A. Sorge, D. Witthaut, and M. Timme, Chaos: An Interdisciplinary Journal of Nonlinear Science **24**, 013123 (2014).
- [36] “The map of the italian high voltage power grid can be seen at the web site of the global energy network institute, namely <http://www.geni.org> and the data here employed have been extracted from the map delivered by the union for the co-ordination of transport of electricity (ucte), <https://www.entsoe.eu/resources/grid-map/>.”.
- [37] M. Komarov, S. Gupta, and A. Pikovsky, EPL (Europhysics Letters) **106**, 40003 (2014).